*Article*

# Types of Xenogenic Olivine from Siberian Kimberlites

**Nikolay S. Tychkov [1],\*, Alexey M. Agashev [1], Nikolay P. Pokhilenko [1], Vladimir A. Tsykh [1] and Nikolay V. Sobolev [1,2]**

[1] Sobolev Institute of Geology and Mineralogy, Siberian Branch of the Russian Academy of Sciences, pr. Akademika Koptyuga 3, 630090 Novosibirsk, Russia; agashev@igm.nsc.ru (A.M.A.); chief@igm.nsc.ru (N.P.P.); tsykh@igm.nsc.ru (V.A.T.); sobolev@igm.nsc.ru (N.V.S.)

[2] Department of Geology and Geophysics, Novosibirsk State University, ul. Pirogova 2, 630090 Novosibirsk, Russia

\* Correspondence: tych@igm.nsc.ru

**Abstract:** This work is devoted to the systematization of the composition of xenogenic olivine from kimberlites as the main mineral composing the lithospheric mantle. Based on data on the composition of olivines from xenoliths and megacrysts from kimberlites, a general division into four types is proposed: olivines of ultrahigh-temperature (HTP-1), high-temperature (HTP-2) and low-temperature (LTP) peridotites, as well as olivines of low-chromium megacryst association (MCA). The separation scheme uses the CaO content as an indicator of the formation temperature and the Mg/(Mg + Fe) ratio as an indicator of the degree of enrichment in olivines. In contrast to Al, the Ca content in olivines from cratonic peridotites is high enough to use only EPMA when applying the proposed scheme. According to this scheme the study of more than 1500 individual olivine xenocrysts from a number of kimberlite bodies of the Siberian platform was made. It revealed three characteristic distributions of olivine types: without high-temperature differences (Obnazhennaya pipe), with significant development of HTP-2 (Olivinovaya and Vtorogodnitsa pipes), and with a significant development of HTP-1 (Dianga pipe). Only the latter type of distribution is characterized by the presence of a noticeable amount of megacryst association olivines. The study of other minor elements ($TiO_2$ and $NiO$) in olivines allowed us to propose a model for the formation of high-temperature olivines of two different types due to the interaction of megacryst melt of various fractionation stages on depleted rocks of the lithospheric mantle. HTP-2 olivines arose upon exposure to a fractionated melt of the late stages of crystallization, and HTP-1 olivines appeared upon exposure to unfractionated (less enriched with incompatible components) megacryst melt at higher temperatures of the initial stage of crystallization.

**Keywords:** olivine; kimberlite; lithospheric mantle; Siberian platform; high-temperature peridotites; megacrysts

## 1. Introduction

Xenoliths carried to the surface by basaltic or kimberlitic melts bear a message from the subcratonic lithospheric mantle (SLM). Mantle xenoliths in kimberlites are of quite rare occurrence for several reasons, including disintegration into xenocrysts during the emplacement. The xenocrysts can provide less precise but more complete information on the SLM structure and on processes at the respective depths. The lithospheric mantle is composed of garnet and spinel peridotites, which contain abundant olivine, one of most widespread kimberlite minerals [1,2]. Olivine would be of interest as an SLM representative, but using its composition as a proxy of SLM features may be problematic: it has

narrower ranges of major elements than garnet, though the variability of minor elements (Ca, Ti, etc.) is sufficient [3,4], and moreover, it can be crystallized directly from kimberlite magma [5–7] or may belong to a megacryst assemblage [8,9].

Currently, considerable attention is paid to the study of olivine, which crystallizes from kimberlite, in order to study the processes of kimberlite formation and the evolution of protokimberlite melts [5–7,10–12]. The study of macrocrysts of xenogenic olivine, which belongs to the depleted rocks of the lithospheric mantle, is given much less attention. This is probably due to the small variety of xenogenic olivine compositions, as well as the lack of clear schemes for its separation into genetic types, which exist, for example, for garnet [13,14] or clinopyroxene [15–17] from kimberlites. Due to this lack of separation schemes, the study of olivines from kimberlites in general cannot provide sufficiently clear information on the composition and structure of the lithospheric mantle, as genetically different types will be mixed, for example, depleted olivine and olivine of low-chromium megacrystal association.

With the development of analytical techniques, it became possible to measure the content of minor elements in olivines, which gave new opportunities for their study and the interpretation of the results [7]. Moreover, methods have been developed by which such studies can be carried out using the relatively affordable Electron Probe Micro-Analyzer (EPMA) [7,18–20]. In a number of recent studies, based on the study of the rare-element composition of olivines from xenoliths of lithospheric mantle rocks, it was shown that different genetic types of olivine differ in composition quite significantly [21,22], which provides the basis for their typification.

The aim of this work is to create a classification scheme for the separation of olivines from kimberlites into their main genetic types, which differ in various composition and characteristics of origin. The presence of such a scheme will make it possible to study in more detail sets of xenocrysts from various kimberlite bodies or alluvial deposits, to compare and identify them also in connection with prospecting problems and assessment of kimberlite diamond grade.

In connection with this aim, a number of problems were solved in the framework of this study. Their consistent implementation corresponds to the structure of the paper described below. After discussion of the standard olivines in Section 2, there is a section that discusses all types of olivines that can be found in kimberlites, including those not belonging to the studied lithospheric mantle rocks, a method for separating such olivines is proposed (Section 3 "Olivine in kimberlites"). In Section 4, "Classification scheme for mantle-derived olivines in kimberlite", based on data on the composition of olivines from xenoliths of mantle rocks of various origins, as well as megacrysts from kimberlites, a developed scheme for the separation of individual olivine crystals by composition into main genetic types is proposed. In Section 5, "Distribution of olivine types in sampled kimberlites", the proposed scheme is used to study the distributions of olivines from several closely located Jurassic kimberlite bodies in the north of the Siberian Platform. Section 6, "Composition of different olivine types", contains information on the compositional characteristics of olivine types from the studied kimberlites and its comparison with olivine compositions from xenoliths of various origins. The origin of the different olivine types is discussed in Section 7. Here, an explanation is offered of the difference in the compositions of the two types of olivines from high-temperature peridotites. Section 8 discusses the characteristic different distributions of xenogenic olivine compositions from kimberlites, their applicability in identifying bodies, and evaluating potential kimberlite diamond grade.

## 2. Materials and Methods

Olivines from four Jurassic pipes—Dianga, Vtorogodnitsa, Olivinovaya, Obnazhennaya (Kuoika kimberlite field, northern Siberian craton)—and one Paleozoic pipe—Aikhal (Alakit kimberlite field, central Siberian craton)—was analyzed using only EPMA, which makes the methods proposed in the work readily available.

EPMA of minor elements in olivine follows methods discussed in [7]. It was performed at the Analytical Center of Multi-Elemental and Isotope Research SB RAS, on a JXA–8230 microprobe (Jeol Ltd) using analyzer crystals TAP (Mg, Al, Si), PET (Ca, Ti, Cr), and LIF (Mn, Fe). Analytical conditions employed were accelerating voltage 20 kV, probe current 250 nA, and spot beam size 1 μm. X-ray intensities of the elements were recorded at the peaks corresponding to Kα lines. Background was measured on both sides of the peak. The signal acquisition time for Si at the peak and background was 20 s; for Mg and Fe, 30 s; for Ca, 120 s; for Ni, 200 s; and for Ti, 240 s. Comparison samples for calculating the concentrations were natural compounds (in parentheses are the comparison samples, average detection limit, and average standard deviation, respectively): Si (olivine (Ch-1), 95.4 ppm, 0.24%); Mg (olivine (Ch-1), 313.2 ppm, 0.20%); Fe (olivine (Ch-1), 54.5 ppm, 0.35%); Ca (blue diopside, 14.1 ppm, 6.9%); Ni ($NiFe_2O_4$, 22.0 ppm, 0.9%); Ti ($TiO_2$, 30.2 ppm, 0.4%).

Olivines from mantle xenoliths and individual olivines from kimberlites studied in the work were taken from the fund of the Laboratory of Lithospheric Mantle and Diamond Deposits of the Institute of Geology and Mineralogy SB RAS, as well as from the personal collections of the authors.

## 3. Olivine in Kimberlites

### 3.1. Olivines Crystallized from Kimberlite Melt

Olivines in kimberlites occur as two main genetic types that differ in size and morphology of crystals: round or irregularly shaped coarse crystals (>0.5 mm) from mantle rocks (xenocrysts) and fine (<0.5 mm) euhedral phenocrysts crystallized from kimberlite magma [23], also referred to as macrocrysts and microcrysts, respectively. According to the work in [24,25], most of the olivine phenocrysts are genetically related to kimberlites, but the most common interpretation is that olivines have xenocrystic core while the phenocrystic material is restricted to narrow rims or micrometer grains [5,10,26,27]. This idea is supported by data from the Udachnaya East kimberlite where phenocrysts are often zoned, with a homogeneous core and a narrow rim (~50 μm) grown from a kimberlite melt [6,7]. Among fine phenocrysts, homogeneous xenocrystic cores are found even in euhedral varieties [7]. Similar correlation between crystal size and origin was discussed in a recent review of [11] who studied olivine xenocrysts from many kimberlites. Therefore, we used only homogeneous cores of >0.5 mm olivines in our study.

### 3.2. Olivines of Cr-Poor Megacryst Assemblage

Some kimberlites, including those described below, enclose numerous olivine crystals with quite low Mg# (Mg/(Mg + Fe) × 100) from 78 to 88 [28,29], and a typical Mg#–CaO composition trend. They hardly can be disintegrated lithospheric mantle rocks since the Mg# ratios are known to be 94–90 for granular peridotite and 94–85.5 for sheared peridotite ([22,29–36] and reference there in). Neither can they be cognate to kimberlite which has a narrow range of Mg# contents from 88 to 93 mol. % [6,7,11,29]. Olivines of this kind were reported from the Monastery kimberlite (South Africa) enclosing abundant coarse (>10 mm) grains of mantle minerals that belong neither to lithospheric mantle residue nor to kimberlite proper [28] and were assigned to a Cr-poor megacryst assemblage (MCA). Compositionally similar but finer olivines are known from other kimberlites as well, interpreted as fine grains or fragments of coarse grains disintegrated during the kimberlite emplacement [24,37].

### 3.3. Peridotitic Olivines

Kimberlites can contain coarse low-temperature or porphyroclastic high-temperature SLM peridotitic xenoliths. High-temperature peridotites are often sheared and bear signatures of secondary enrichment upon reaction with asthenospheric melts. The peridotite that experienced secondary enrichment no longer represents the primary depleted subcratonic lithosphere: the average characteristics of the genetically mixed mineral assemblage will depend on percentages of mixing rather than on properties of different mantle lithologies.

## 4. Classification Scheme for Mantle-Derived Olivines in Kimberlite

### 4.1. Craton Peridotitic, Megacrystic, and Magmatic Olivines

Megacrystic olivines were discriminated from peridotitic olivines with reference to data on 230 peridotite xenoliths from twelve kimberlites of the North American, South African, and Siberian cratons [22,30–36,38,39].

Figure 1 shows the compositions of olivines from peridotites (circles) in comparison with olivines of the low-chromium megacryst association, and a separation line is proposed for interpreting the origin of xenocryst from kimberlites. On the example of the composition of xenocryst from kimberlites Colossus (Zimbabwe) [29], Figure 2, it can be seen that olivines of these two genetic groups can be equally represented in kimberlites. The authors of [8,29] discuss the composition of olivine xenocrysts from Colossus kimberlites, and it is suggested that the olivine group with a high Mg# > 89 and CaO > 0.05 wt.% refers not to peridotites, but to highly chromic megacrystic minerals associations crystallizing from unfractionated melt. Indeed, these olivines are very close in chemistry to the high magnesian part of the trend of olivine megacrysts. However, based on the fact that kimberlites of different ages and location contain xenoliths of mantle rocks with such high-magnesian and high-calcium olivines, we propose to classify them as products of the disintegration of high-temperature peridotites. As will be shown below, these peridotites are indeed closely genetically related to megacrystic olivines, which crystallized from the least fractionated melt. Two varieties of olivine megacrystals reaching a size of 10 cm are distinguished in the kimberlites of the Udachnaya pipe. The first refers to the usual low-chromium megacrystal association with relatively low magnesium number. The second is characterized by a high magnesian number of ~93. Studies by Pokhilenko et al. [40] unequivocally show that the latter has a CaO content of less than 0.02 wt.% and refers to disintegrated megacrystalline pyrope harzburgite-dunites. Their composition is shown in Figure 1 as triangles.

Foley [41] showed that olivines of magmatic origin (basalts of oceanic islands, picrites, continental alkaline, plume-related continental rocks, etc.) can be separated from olivines from peridotites of ancient cratons by CaO content of approximately 700 ppm (or 0.098 wt.%). Olivines of some of the listed rocks (for example, continental flood-basalts of Siberian platform) can get into kimberlites as xenogenic material if during intrusion the kimberlite passed through an already existing body contains magmatic olivine, but it seems to us, this is a very rare case. The probability of seeing magmatic olivines increases significantly if we study olivines not directly from kimberlite, but from alluvial deposits. In this regard, within the framework of our classification, we propose to limit the field of olivines from cratonic peridotites to the level of 0.11 wt.% CaO (786 ppm), which is slightly more than Foley et al. [41] suggests, but correlates with the observed existence of such calcium olivines from the Kaapvaal craton kimberlites (Figure 1).
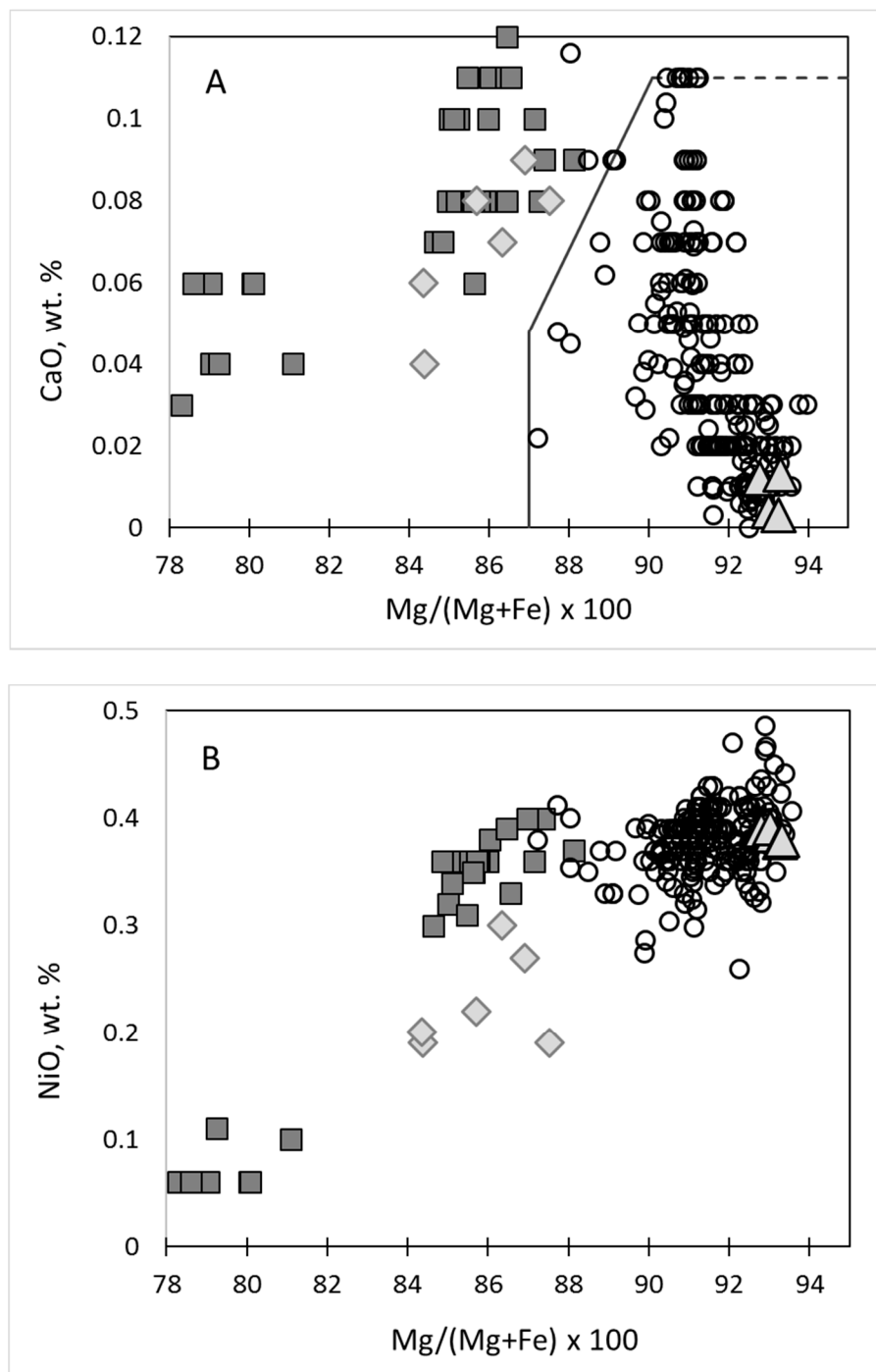
**Figure 1.** Division boundary (solid line) between low-Cr olivine megacrysts from kimberlite (squares and diamonds stand for Monastery [28] and Jagersfontein [9] kimberlites, respectively) and olivines from 230 peridotitic xenoliths (circles) from different kimberlites [22,30–36,38,39]. The dotted line separates high-Ca magmatic olivine [41]. Triangles are olivines from megacrystalline pyrope peridotites from Udachnaya [40,42], shown for comparison with low-Cr megacryst assemblage.
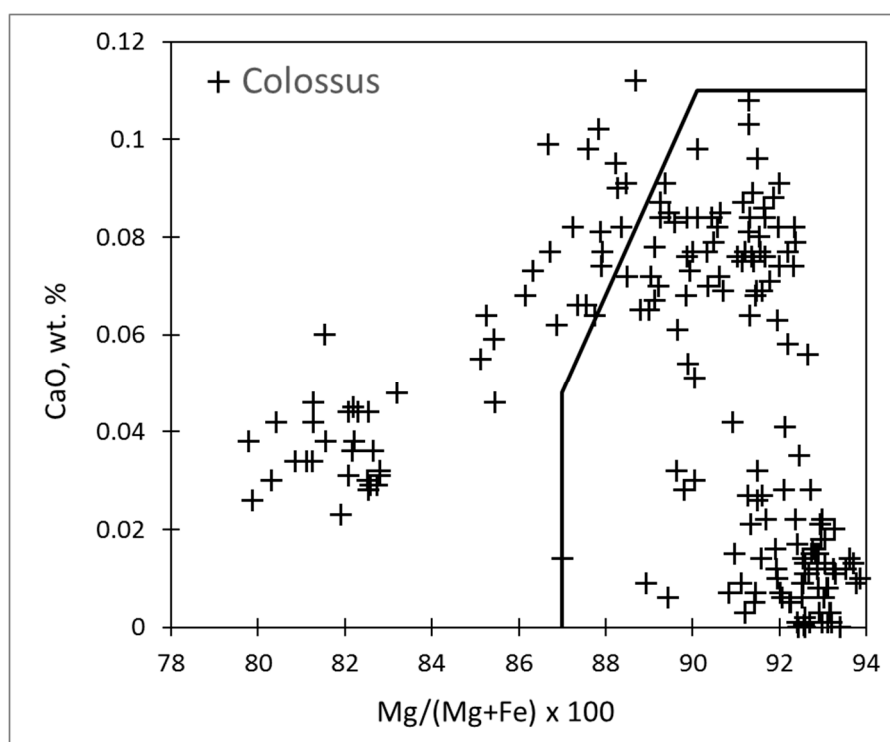
**Figure 2.** Olivine xenocrysts from Colossus kimberlites, Zimbabwe. Data from work in [29]. Solid line is the boundary between low-Cr megacryst and peridotitic olivines.

## 4.2. Different Olivines from Peridotites

As it was shown by the analysis of experimental and natural peridotitic systems, the incorporation of Ca into the structure of olivine [43] is sensitive to temperature [44], which allows preliminary discrimination between olivines from high- and low-temperature peridotites. The precision of the classical electron microprobe analysis is unsuitable for Ca-in-Ol thermometry [18,22], but EMPA can be used for general statistical division into main genetic types. Figure 3 demonstrates the dependence of CaO contents in olivine determined by the standard EMPA routine on temperature calculated using standard thermometers [45,46] from peridotitic xenoliths in South African and North American kimberlites.

Olivines in low-temperature peridotite (LTP) that form at <1100 °C contain ~0.025 wt.% CaO, whereas those from high-temperature peridotite have large ranges of CaO contents (0.025–0.120 wt.%) and crystallization temperatures (1100–1450 °C). The Zimbabwe Colossus kimberlite (Figure 2), as well some other kimberlites [12], contain a group of peridotitic olivines with >0.05 wt.% CaO. It is reasonable to consider peridotitic olivines with >0.050 wt.% CaO, which crystallize at >1300 °C, as a separate group of ultrahigh-temperature peridotites (HTP-1), and peridotitic olivines with 0.025–0.050 wt.% CaO, which crystallize at 1100–1300 °C, as high-temperature peridotites (HTP-2). Thus, there are three temperature groups of olivines consistent with the classical division.

The suggested temperature division of peridotitic olivines is applicable solely to xenoliths from Precambrian cratons with low heat flux (~35–45 mW/m$^2$), as the Ca content in olivine is inversely proportional to pressure [43]. For instance, olivines from granular lherzolite and harzburgite of the West Sangilen [47] lithospheric mantle (Central Asian orogenic belt) contain 0.06–0.12 wt.% CaO at a properly estimated equilibrium temperature of 960–1060 °C. The lithospheric mantle heat flux of the West Sangilen area exceeds 90 mW/m$^2$, as in Northwestern Spitzbergen [48].
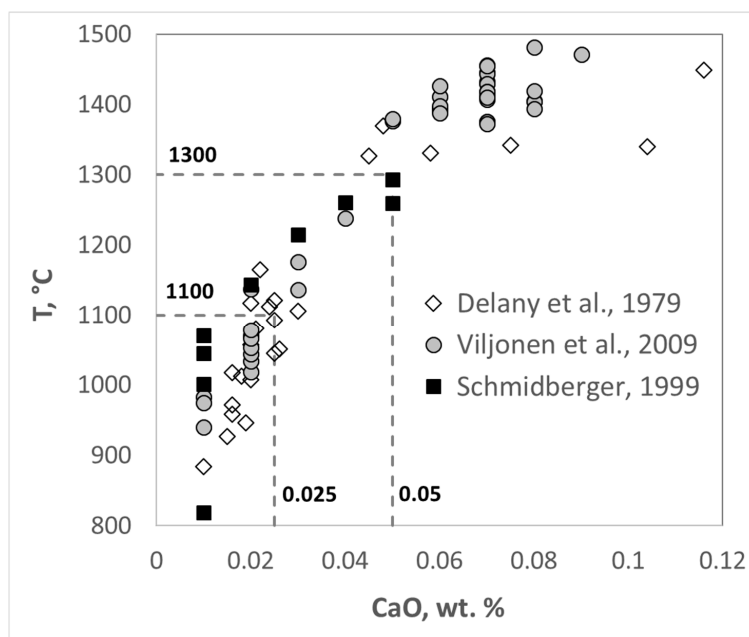
**Figure 3.** Temperature dependence of CaO in peridotitic olivine. The symbols stand for olivines from different sites: rhombs = Bultfontein Floors, Frank Smith mine, Matsoku (S. Africa) [30]; circles = Premier diamond mine (S. Africa) [35]; squares = Somerset Island kimberlites (N. America) [32].

## 5. Distribution of Olivine Types in Sampled Kimberlites

The distribution of olivine compositions in several kimberlite pipes was analyzed using the suggested classification in order to see the differences in distribution between kimberlites of one field and to characterize the mineral chemistry and origin of different types of xenolithic (xenocrystic) olivine. We sampled four Jurassic pipes in the Kuoika kimberlite field (northern Siberian craton): Dianga, Vtorogodnitsa, Olivinovaya, and Obnazhennaya (Figure 4). According to previous results [17,49–52], the four kimberlites, which differ in the types and chemistry of mantle minerals and in diamond grade, represent the mineralogical diversity of a certain stage of kimberlite magmatism in a specific area. The Dianga kimberlite, the deepest pipe in the field, bearing diamonds, unlike the other pipes, and is the only one with its estimated PT conditions [17,49] mainly outside the diamond stability field. Unlike Dianga, the Vtorogodnitsa and Olivinovaya kimberlites carry minerals from both low-temperature and high-temperature peridotites, but fall totally beyond the conditions of diamond stability. The Obnazhennaya pipe is among the shallowest kimberlites of the field, and its mineralogy is restricted to that of low-temperature granular peridotite and pyroxenite [53,54].

The distribution of olivine types in the four kimberlites (Table 1, Figure 5) is similar in the Vtorogodnitsa and Olivinovaya pipes and may be typical of the kimberlite field as a whole: few sporadic grains of MCA and HTP-1 olivines and approximately similar percentages of the HTP-2 and LTP types. The Dianga kimberlite contains well-represented olivines of all four types, and HTP-1 olivines are markedly more abundant than the HTP-2 varieties. A similar distribution of olivine types was reported from two more kimberlites in other areas: the Neoproterozoic Colossus pipe (Figure 2) from the Zimbabwe craton, Zimbabwe [29], and the Triassic Malaya Kuonapka kimberlite from the Kuranach field in Yakutia [12]. Thus, xenolithic olivines in kimberlites of different ages appear to be distributed in two ways: (i) markedly greater percentages of HTP-1 than HTP-2 olivines and quite large amounts of the MCA type (Dianga, Colossus, and Malaya Kuonapka kimberlites) and (ii) high percentages of HTP-2 and almost lacking HTP-1 (and MCA) olivines (Vtorogodnitsa and Olivinovaya kimberlites); olivines from low-temperature peridotite reach quite large percentages (30–50%). Both distributions may be present in coeval kimberlites within one area, as in the case of the Kuoika field. Shallow tipe pipe Obnazhennaya, also present in the Kuoika field, bears only LTP olivines.
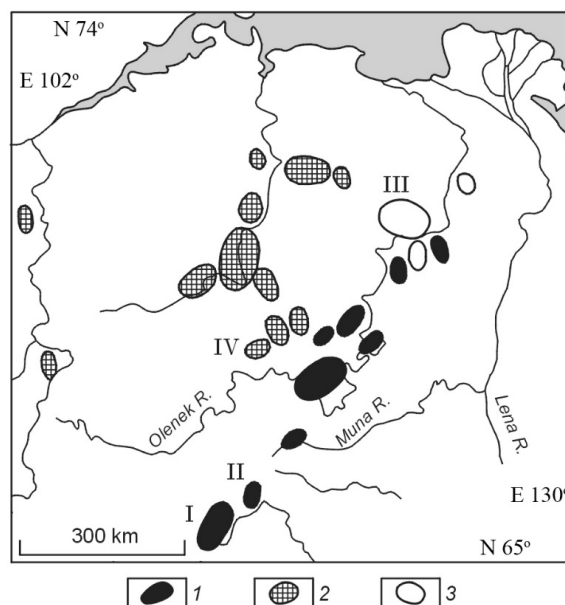
**Figure 4.** Location map of the northeastern Siberian craton, with kimberlite fields of different ages: 1, PZ (S–D, D–C); 2, MZ (T); 3, MZ (J). Roman numerals stand for their names: I, Daldyn (with Udachnaya pipe); II, Alakit (with Aikhal pipe); III, Kuoika (with Dianga, Vtorogodnitsa, Olivinovaya and Obnazhennaya pipes); IV, Kuranakh (with Malaya Kuonapka pipe).
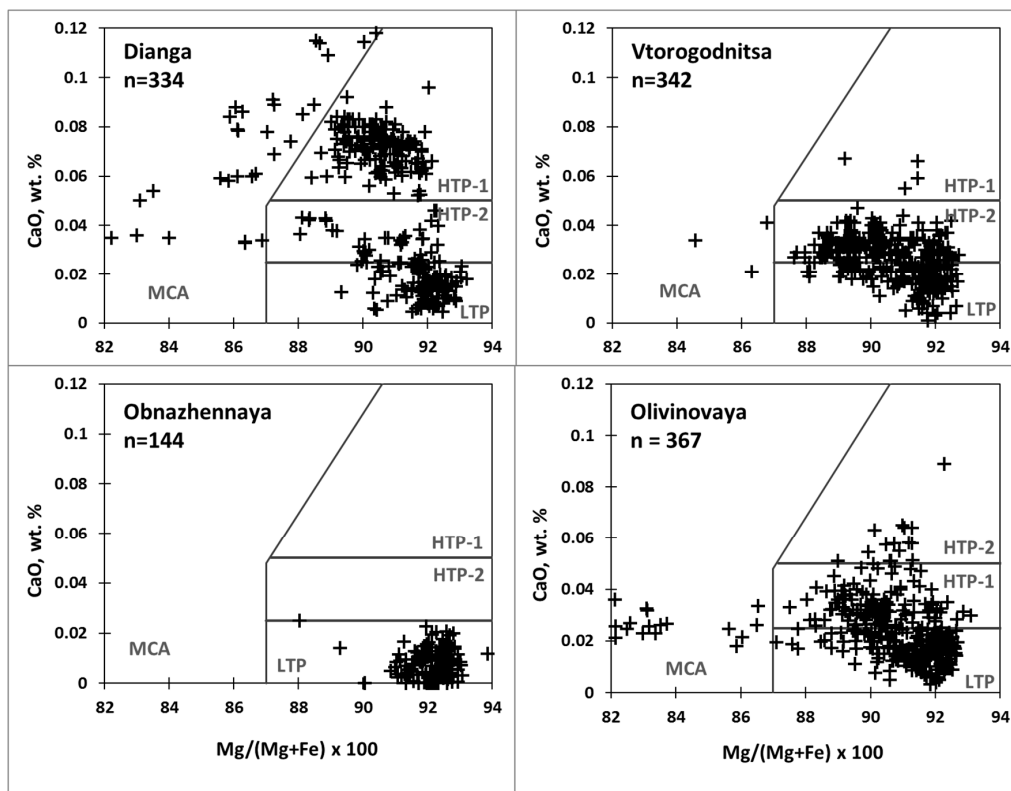


**Figure 5.** Pluses (+) are compositions of xenolithic olivines from kimberlites in the Siberian craton. Contoured fields represent different olivine types: MCA = low-Cr megacryst assemblage, LTP = low-temperature peridotites < 1100 °C, HTP-1 = high-temperature peridotite > 1300 °C, HTP-2 = high-temperature peridotite 1100–1300 °C. n is number of analyzed grains. See supplementary Table S1.

**Table 1.** Xenolithic olivines of different types: percentages in different kimberlites. Colossus kimberlites data from work in [29]. Symbols for kimberlite types are same as in Figure 5. n is number of analyzed grains.

| Kimberlite | MCP | HTP-1 | HTP-2 | LTP | n |
|---|---|---|---|---|---|
| Obnajennaya | 0 | 0 | 0 | 100 | 110 |
| Vtorogodnitsa | 1 | 1 | 56 | 42 | 342 |
| Olivinovaya | 1 | 5 | 42 | 52 | 88 |
| Dianga | 10 | 46 | 12 | 32 | 334 |
| Colossus | 29 | 30 | 6 | 34 | 209 |

## 6. Mineral Chemistry of Olivines of Different Types

Variations of some major oxides in olivines from the four kimberlites in the northern Siberian craton (Figure 6; Table 2) are characterized below according to the distinguished types.

**Table 2.** Composition variations in olivine groups distinguished according to texture and formation temperature of peridotite: granular or sheared, after work in [7,11] and LTP or HTP-1 + HTP-2 (this study), respectively. HTP-1 and HTP-2 are two subtypes of high-temperature peridotites and belong to one group.

| Types | Mg# | NiO | CaO | TiO$_2$ |
|---|---|---|---|---|
| Granular | 87.8–94.0 | 0.26–0.48 | 0–0.092 | 0–0.008 |
| LTP | 89.8–93.1 | 0.34–0.42 | 0–0.025 | 0–0.022 |
| Sheared | 86.0–92.2 | 0.22–0.42 | 0.032–0.091 | 0.017–0.050 |
| HTP-1 + HTP-2 | 88.0–92.5 | 0.19–0.40 | 0.025–0.089 | 0.008–0.041 |
| MCA | 80.0–90.0 | 0.10–0.38 | 0.022–0.10 | 0.011–0.040 |

Olivines of the Cr-poor megacryst assemblage (MCA) are abundant in Dianga kimberlite: large ranges from >90 Mg#, >0.38 wt.% NiO, and <0.01 wt.% TiO$_2$ typical of depleted cratonic lithospheric mantle to enriched compositions with < 80 Mg#, <0.1 wt.% NiO, and >0.04 wt.% TiO$_2$. The compositions form direct relationship (e.g., in the Mg#–NiO coordinates) that record fractional crystallization of mantle silicate melts.

Low-temperature peridotite (LTP) olivines: narrow ranges of Mg# (89.8–93.1), NiO (0.34–0.42 wt.%), and 0.022 wt.% TiO$_2$ in 90% of cases, which correspond to depleted cratonic lithospheric mantle (granular lherzolite and harzburgite-dunite).

High-temperature peridotite (HTP-1 and HTP-2) olivines: intermediate between LTP and MCA olivines. The contents of TiO$_2$ and NiO cover the full range of compositions from ultradepleted to enriched, whereas the lower Mg# bound (86–87) is higher than Mg# in MCA olivines.

The compositions of different olivine types were discussed in the literature Ref [5,7,11,12,21,22,24,28,29,34,42], but more often in terms of texture (granular or sheared) rather than formation temperature of peridotites. Granular peridotite mainly forms at low temperatures, whereas the sheared counterpart is most often of high-temperature origin (Table 2), though this division is not very strict.

The compositions of LTP and HTP-2 olivines generally correspond to those of granular and sheared peridotites, respectively. The temperature-based olivine types do not differ much in the contents of major oxides, possibly because the samples are from only four pipes of the whole kimberlite field, but the variations in CaO, which are used as a temperature proxy, are distinct. The contents of CaO in olivines from granular peridotite correspond to a crystallization temperature of 1400 °C. Many granular peridotites are of high-temperature origin because some high-temperature peridotites escape deformation and some sheared rocks experience later annealing and recrystallization. Many granular peridotites known from the Udachnaya kimberlite in Yakutia have high crystallization temperatures

and bear signatures of annealing and recrystallization recorded in the morphology of garnets occurring as coarse (up to 5 mm), often sheared, grains [55–57].
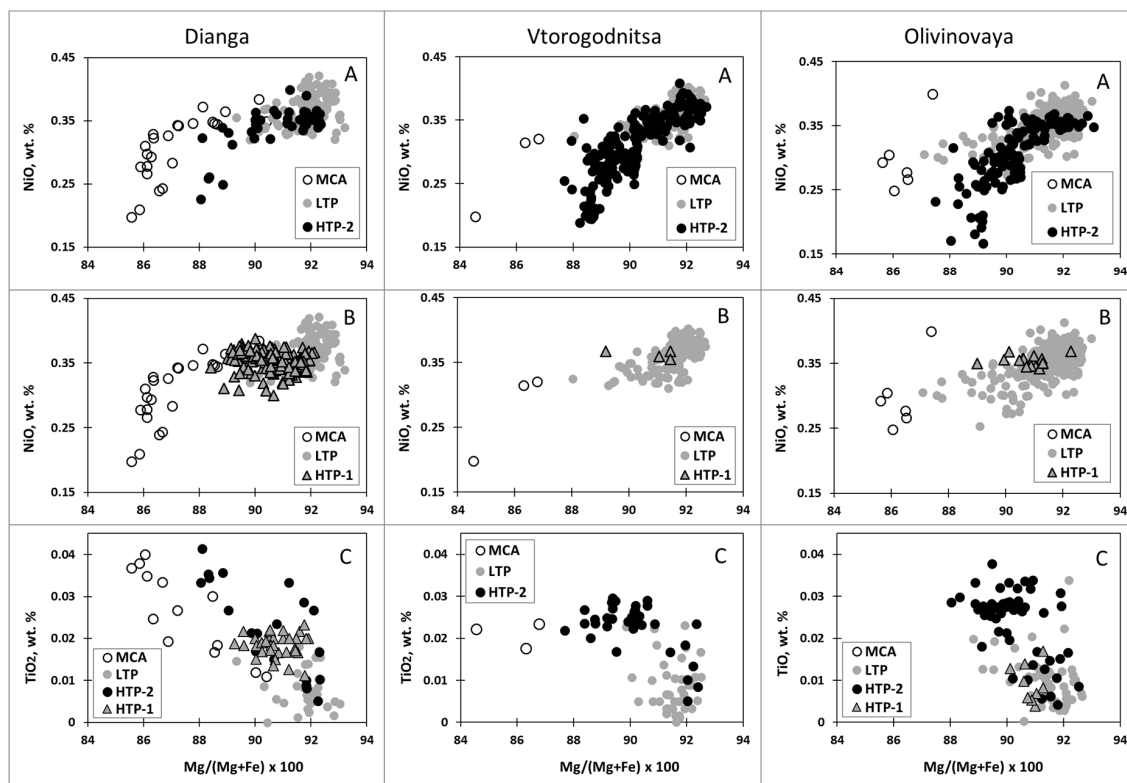


**Figure 6.** Distribution of olivines from kimberlites in northern Siberian craton. Olivine types: open circles = MCA, gray circles = LTP, black circles = HTP-2, triangles = HTP-1. Row (**A**) shows HTP-2 olivines in comparison to LTP and MCA; Row (**B**) shows the same for HTP-1; Row (**C**) define Mg#-TiO$_2$ for all types. First column—Dianga, second—Vtorogodnitsa, third—Olivinovaya kimberlites. See supplementary Table S1.

The LTP and HTP-1 olivines show generally lognormal distributions of the oxides, but the HTP-2 olivines have two peaks in Mg# and NiO (Figure 7). One peak (high MgO and NiO at low TiO$_2$) has the same position as that for LTP and corresponds to depleted rocks, whereas the other is shifted to lower MgO and NiO at higher TiO$_2$ contents and represents more enriched mantle. Thus, there are depleted and enriched composition subtypes within the HTP-2 type distinguished on the basis of temperature. The two subtypes are divided according to thresholds of 91.5 Mg#, 0.315 wt.% NiO, and 0.016 wt.% TiO$_2$. The threshold values may be slightly higher or lower in kimberlites that sample a lithosphere with different parameters.

Unlike the HTP-2 variety, the HTP-1 olivines have more uniform compositions than those from depleted SLM (Figure 7). At the same time, they have intermediate Mg#, NiO, and TiO$_2$ values between the depleted (LTP) and enriched (HTP) compositions (see histograms in Figure 7): the TiO$_2$ peaks correspond to 0.006 wt.% in LTP, 0.026 wt.% in HTP, and 0.014 wt.% in HTP-1. The Ti peak for LTP olivines is not far above the detection limit of our EPMA analyses. Such a Ti content in LTP olivines can be interpreted as its almost complete absence. In this regard, we consider this point not critical for our study. The difference between the HTP-2 and HTP-1 olivines may record the specificity of peridotite formation at different temperatures.
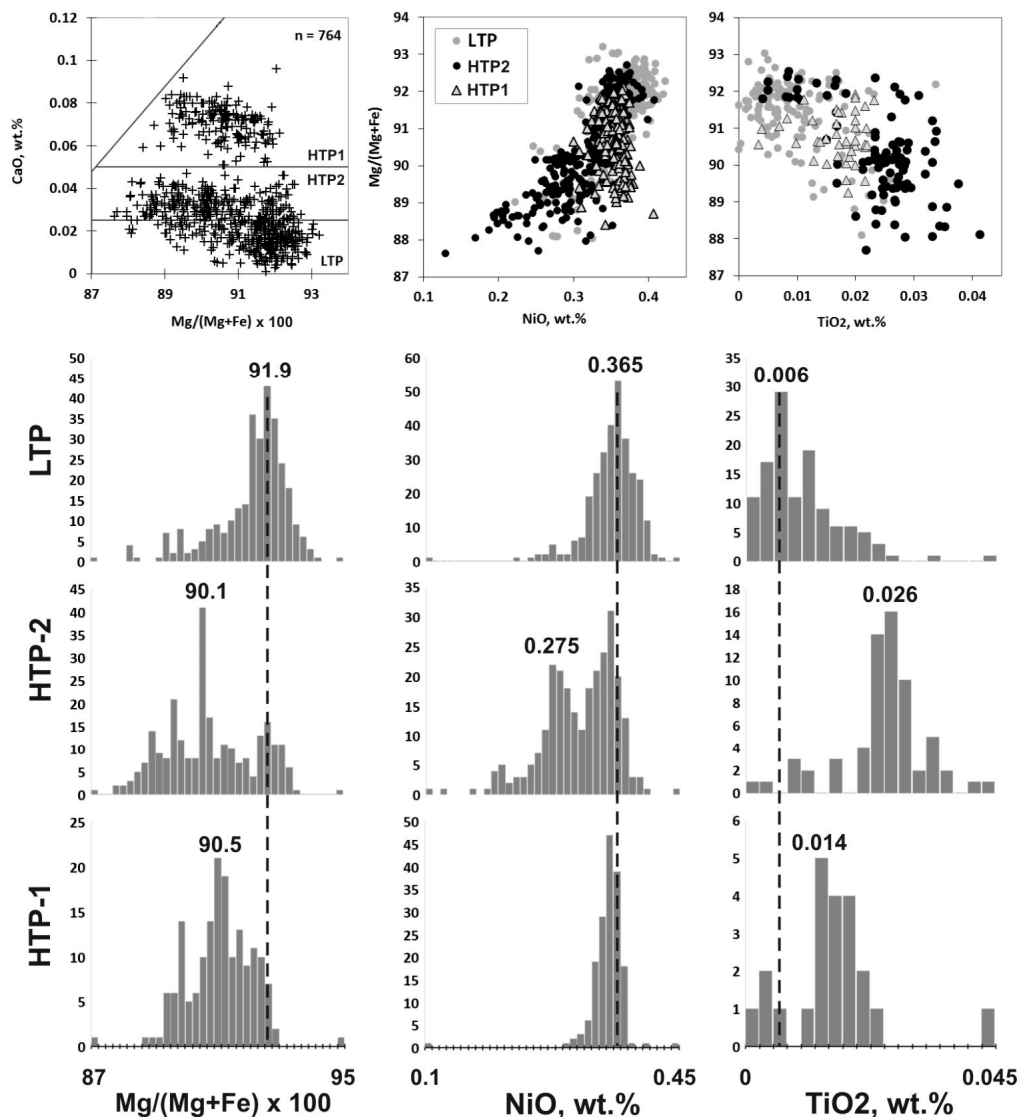
**Figure 7.** Distribution of some major oxides in olivines of different types. Olivine types: open circles = MCA, gray circles = LTP, black circles = HTP-2, triangles = HTP-1. Scale spacing in histograms: 0.2 for Mg/(Mg + Fe) × 100, 0.01 wt.% for NiO, and 0.0025 wt.% for $TiO_2$. Dashed lines mark peak values in low-temperature peridotites (LTP) corresponding to depleted compositions.

## 7. Origin of Different Olivine Types

The contents of CaO, NiO, and $TiO_2$ in xenolithic olivines of different types are plotted in Figure 6 as a function of Mg/(Mg + Fe) × 100, and are especially well representative in the Dianga kimberlite. HTP-2 olivines plot a typical trend of secondary enrichment with Mg# and NiO lower than in LTP olivines mostly found in depleted rocks (Figure 6A). The enrichment trend is less prominent in the HTP-1 variety (Figure 6B): decreasing Mg#, but no NiO decrease. The $TiO_2$ contents (Figure 6C) are higher in HTP-2 than in LTP olivines and increase from below detection to 0.04 wt.% (the maximum level reached by MCA olivines), whereas the Mg# content decreases. HTP-1 olivines contain slightly more $TiO_2$ than the LTP type (at the level of minimum $TiO_2$ in MCA olivine). Thus, there are two temperature-controlled types of secondary enrichment in olivines associated with the formation of high-temperature peridotites.

Megacrystic minerals were attributed to fractional crystallization of asthenospheric melts [9,37,58–60] proceeding from their composition trends that trace the evolution of the growth medium. Studies of different types of xenoliths and megacryst minerals from the Jagersfontein

kimberlite in the Kaapvaal craton in South Africa led Burgess and Harte [61,62] to the conclusion that high-temperature enriched peridotites from different depths interacted with silicate melts of different compositions. In the deepest lithosphere, they were less enriched MORB-type (Mid-Ocean Ridge Basalts) melts, whereas the shallower depleted peridotite was affected by more enriched melts. The difference in melt enrichment degrees was explained [61,62] by progressive fractional crystallization of Cr-poor megacrysts. The enrichment of residual SLM sampled by the kimberlites from the northern Siberian craton was likely controlled by interaction with melts that lost different amounts of compatible elements during fractional crystallization.

The origin of olivines in the analyzed kimberlites is illustrated in Figure 8 with the example of the Dianga pipe. Two populations of megacrysts (MCA-1 and MCA-2) correspond to different ends of the fractional crystallization [63,64] series. MCA-1 formed from a melt with lower contents of incompatible elements than that for MCA-2. HTP-1 olivines may result from the interaction of the depleted lower lithosphere with poorly enriched melts that also crystallized MCA-1 olivines, because the enrichment of LTP during the formation of HTP-1 remained within the limits of the MCA-1 olivines. HTP-2 olivines, in their turn, bear an effect of more enriched melts that produced MCA-2 olivines or intermediate melts: the $TiO_2$ and NiO contents in HTP-2 olivines reach, but do not exceed, the values for those from MCA-2. HTP-1 olivines, found often in the Dianga pipe, most deeply rooted one in the Kuoika field, must be transported from the greatest depths.
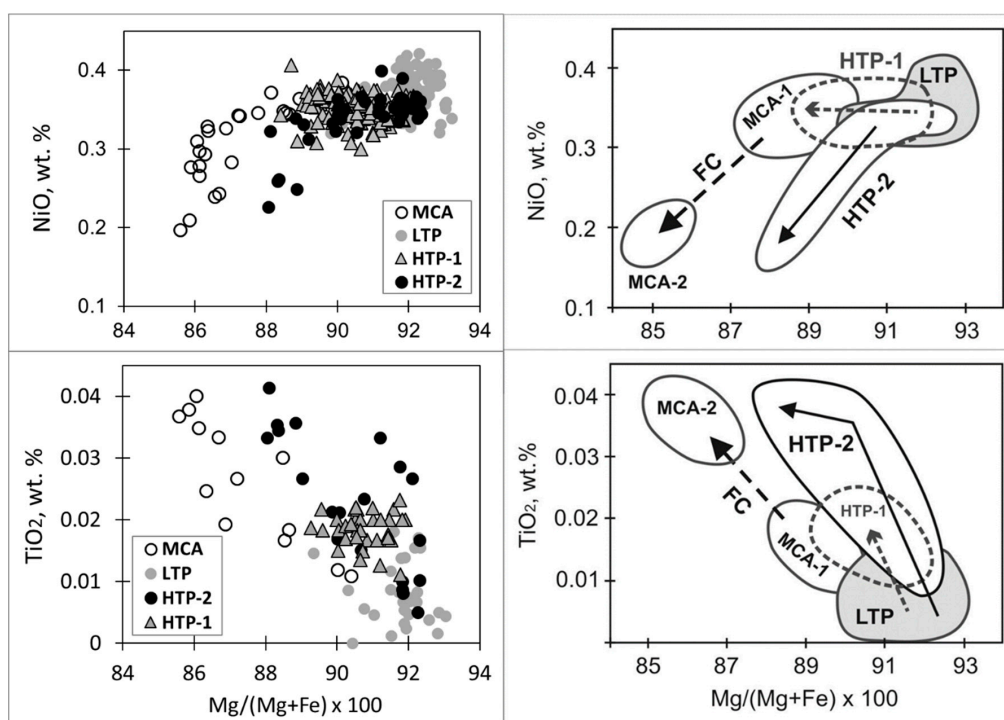


**Figure 8.** Origin of olivines in kimberlites from the northern Siberian craton: olivines from the Dianga kimberlite (left) and a model of their formation (right). Olivine types: MCA-1 and MCA-2 are early and late low-Cr megacrysts, respectively; LTP = low-temperature lherzolite < 1100 °C, HTP-1 = high-temperature peridotite > 1300 °C, HTP-2 = high-temperature peridotite 1100–1300 °C; FC = fractional crystallization of low-Cr megacryst olivines.

The situation would correspond to the model of lower lithosphere enrichment by a rising evolving "megacrystic" melt [58,61,62]. However, a reasonable objection to this model may be that both Ti and Fe are higher in the later MCA-2 than in the earlier MCA-1 crystals, contrary the expectation of low Ti and Fe in the latest fractionated melt after crystallization of high-Ti and high-Fe phases (mainly ilmenite and garnet). In terms of temperature, the evolution of the megacrystic melt would be inverse: the earlier

HTP-2 varieties produced by the action of this melt would have higher origin temperatures than HTP-1 olivine. This interpretation is, however, inconsistent with the >0.05 wt.% CaO contents in olivines from xenoliths that originated at >1300 °C, as estimated from polymineral thermobarometry [46,65], etc.; i.e., the CaO contents in olivines show positive correlation with equilibrium temperatures (Figure 3).

The contradiction may be explained by assuming that MCA-2 olivines actually crystallized from the latest melt of the first crystallization step, prior to the formation of ilmenite, rather than from the latest megacrystic melt. Studies of ilmenite and silicates from the Monastery kimberlite in South Africa [59] revealed five steps in the sequence of crystallization from the megacrystic melt (Figure 9): oliv + opx + cpx + gnt (1), cpx + gnt + opx + ilm (2), phlog + ilm (3), zircon + phlog + ilm (4), and zircon + Fe-oliv + phlog + ilm (5). Thus, olivine crystallizes at the first (before ilmenite) and high-Fe fifth steps. Olivine megacrysts from the Monastery kimberlite [37], with the composition trend corresponding to the crystallization sequence of Moore et al. [59], shows less Ti in the latest olivines with greater Fe contents and lower Mg# (~79) than in the more magnesian (Mg# 84–88) olivines of step 2 (Figure 9). The fractional crystallization sequence from MCA-1 to MCA-2 in the Dianga kimberlite occurs within step 1 of the model of Moore et al. [59] in the Mg# range from 85 to 90.5, with positively correlated Ti and Fe, as in the case of the Monastery kimberlite. The Dianga kimberlite contains only step-1 megacryst olivines.

Yet, the model fails to explain some essential features. Apparently, the crystallization of olivine from a megacrystic melt and the formation of compositionally diverse olivines enclosed in high-temperature peridotide are complicated and require additional investigation with reference to a greater number of trace elements.
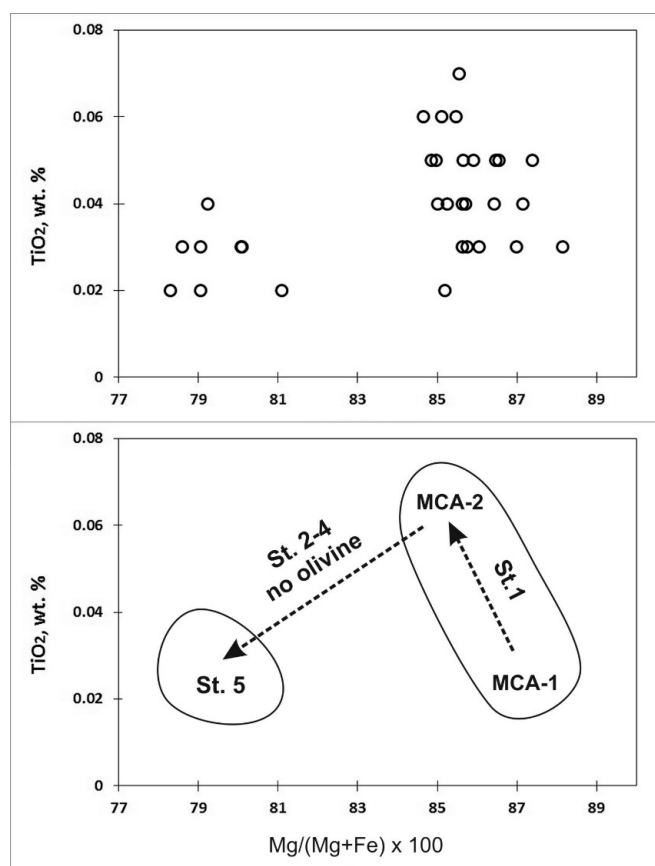


**Figure 9.** Crystallization of olivine from megacrystic melt in Monastery kimberlite (S. Africa), after the model of Moore [59]. Circles are olivine megacrysts from Monastery kimberlite (data from work in [37]). Crystallization steps: 1 = **oliv** + opx + cpx + gnt, 2 = cpx + gnt + opx + ilm, 3 = phlog + ilm, 4 = zircon + phlog + ilm, 5 = zircon + **Fe-oliv** + phlog + ilm.

## 8. Discussion and Conclusions

Xenolithic (xenocrystic) olivines in kimberlites can be divided into four main genetic types. Olivines of the Cr-poor megacryst assemblage (MCA) differ from peridotitic olivines in the Mg# vs. CaO relationship. Peridotitic olivines are further divided into low-temperature, high-temperature, and ultrahigh-temperature peridotite varieties according to temperature-dependent CaO contents. The suggested division is supported by log-normal distributions of major oxides within the distinguished types of peridotitic olivines. HTP-2 olivines show bimodal element distributions and are of two subtypes corresponding, respectively, to unaltered lithospheric mantle and to material that underwent secondary enrichment during the formation of high-temperature peridotite.

The analyzed kimberlite samples from the northern Siberian craton differ in the amount of olivine types they host: HTP-2 olivines are absent from the Obnazhennaya pipe, but are abundant, along with the HTP-1 varieties, in the Olivinovaya and Vtorogodnitsa kimberlites; MCA olivines reach notable amounts in the Dianga pipe. The percentages of HTP-2 and HTP-1 are not equal in any of the kimberlites, possibly because they uptake lithospheric mantle of different depths and features. The Dianga kimberlite samples the deepest lithosphere, as well as the diamond-rich Malaya Kuonapka kimberlite from the Kuranakh field which has similar element distributions in olivines [12]. The kimberlites containing MCA olivines and predominant HTP-1 olivines are commonly most deeply rooted in a field. On the other hand, they not necessarily should bear diamond: the deepest MCA and HTP-1 material cannot be diamondiferous, and its uptake reduces the diamond potential of a pipe. However, only the deepest kimberlites could capture material below the graphite–diamond phase boundary in the case of thick cratonic lithosphere [17,49], which explains the presence of diamonds in the Kuoika and Kuranakh kimberlite fields. The Middle Paleozoic lithosphere of the northern Siberian craton sampled by kimberlites in the Alakit and Daldyn fields is much thicker than the Mesozoic lithosphere [17]. The richest Aikhal kimberlite from the Alakit field contains mainly LTP and HTP-2 olivines and almost lacks the MCA and HTP-1 varieties (Figure 10), like the Olivinovaya and Vtorogodnitsa kimberlites. It would be reasonable to expect some diamond potential from kimberlites in areas of thicker lithosphere, which show olivine composition patterns similar to those in these two pipes, where lithospheric mantle material was uptaken at shallower depths.
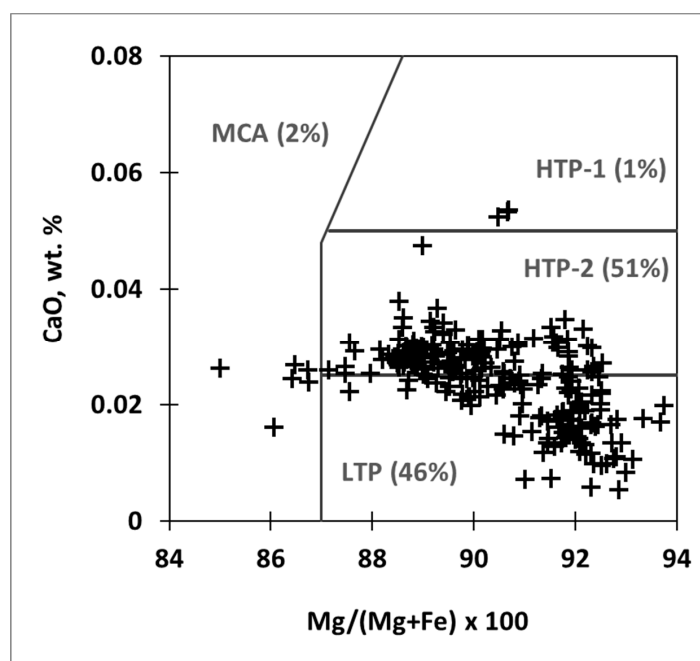


**Figure 10.** Pluses are compositions of olivines from Aikhal kimberlite (Alakit kimberlite field, central Siberian craton). Note, that MCA = 2%. See supplementary Table S1.

## References

1. Nixon, P.H. *Mantle Xenoliths*; Wiley: New York, NY, USA, 1987.
2. Pearson, D.G.; Canil, D.; Shirey, B. Mantle Samples Included in Volcanic Rocks: Xenoliths and Diamonds. In *The Mantle and Core: Treatise on Geochemistry*; Elsevier: New York, NY, USA, 2003; Volume 2, pp. 171–275.
3. Mitchell, R.H. Composition of olivine, silica activity and oxygen fugacity in kimberlite. *Lithos* **1973**, *6*, 65–81. [CrossRef]
4. Mitchell, R.H. *Kimberlites: Mineralogy, Geochemistry and Petrology*; Plenum Press: New York, NY, USA, 1986; 442p.
5. Arndt, N.T.; Guitreau, M.; Boullier, A.-M.; Le Roex, A.; Tommasi, A.; Cordier, P.; Sobolev, A. Olivine and the origin of kimberlite. *J. Petrol.* **2010**, *51*, 573–602. [CrossRef]
6. Kamenetsky, V.S.; Kamenetsky, M.B.; Weiss, Y.; Navon, O.; Nielsen, T.F.D.; Mernagh, T.P. How unique is the Udachnaya-East kimberlite? Comparison with kimberlites from the Slave Craton (Canada) and SW Greenland. *Lithos* **2009**, *112*, 334–346. [CrossRef]
7. Sobolev, N.V.; Sobolev, A.V.; Tomilenko, A.A.; Kovyazin, S.V.; Batanova, V.G.; Kuz'min, D.V. Paragenesis and complex zoning of olivine macrocrysts from unaltered kimberlite of the Udachnaya-East pipe, Yakutia: Relationship with the kimberlite formation conditions and evolution. *Russ. Geol. Geophys.* **2015**, *56*, 260–279. [CrossRef]
8. Moore, A.; Belousova, E. Crystallization of Cr-poor and Cr-rich megacryst suites from the host kimberlite magma: Implications for mantle structure and the generation of kimberlite magmas. *Contrib. Mineral. Petrol.* **2005**, *149*, 462–481. [CrossRef]
9. Hops, J.; Gurney, J.J.; Harte, B. The Jagersfontein Cr-poor megacryst suite—Towards a model for megacryst petrogenesis. *J. Volcanol. Geotherm. Res.* **1992**, *50*, 143–160. [CrossRef]
10. Brett, R.C.; Russell, J.K.; Moss, S. Origin of olivine in kimberlite: Phenocryst or imposter. *Lithos* **2009**, *1125*, 20–212. [CrossRef]
11. Giuliani, A. Insights into kimberlite petrogenesis and mantle metasomatism from a review of the compositional zoning of olivine in kimberlites worldwide. *Lithos* **2018**, *312–313*, 322–342. [CrossRef]
12. Sobolev, N.V.; Sobolev, A.V.; Tomilenko, A.A. Unique compositional peculiarities of Olivine Phenocrysts from the post flood basalt diamondiferous Malokuonapskaya Kimberlite Pipe, Yakutia. *Dokl. Earth. Sci.* **2015**, *463*, 828–832. [CrossRef]
13. Sobolev, V.S.; Nai, B.S.; Sobolev, N.V.; Lavrent'ev, Y.G.; Pospelova, L.N. Xenoliths of diamond-bearing pyrope serpentinites from the Aikhal kimberlite, Yakutia. *Dokl. Akad. Nauk SSSR* **1969**, *188*, 1141–1143.
14. Schulze, D.J. A classification scheme for mantle-derived garnets in kimberlite: A tool for investigating the mantle and exploring for diamonds. *Lithos* **2003**, *71*, 195–213. [CrossRef]
15. Ramsay, R.R.; Tompkins, L.A.; Meyer, H.O.A.; Leonardos, O.H. The geology, heavy mineral concentrate mineralogy, and diamond prospectivity of the Boa Esperanca and Cana Verde pipes, Corrego D'anta, Minas, Brazil. In *Proceedings of the 5th International Kimberlite Conference*; Companhia de Pesquisa de Recursos Minerais: Brasilia, Brazil, 1994; Volume 1, pp. 329–345.

16.　Nimis, P.; Taylor, W.R. Single clinopyroxene thermobarometry for garnet peridotites. Part I. Calibration and testing of a Cr-in-Cpx barometer and an enstatite-in-Cpx thermometer. *Contrib. Mineral. Petrol.* **2000**, *139*, 541–554. [CrossRef]

17.　Tychkov, N.S.; Yudin, D.S.; Nikolenko, E.I.; Sobolev, N.V. Mesozoic lithospheric mantle of the north-eastern part of the Siberian Platform according to the data of minerals from kimberlites. *Russ. Geol. Geophys.* **2018**, *59*, 1254–1270. [CrossRef]

18.　Korolyuk, V.N.; Pokhilenko, L.N. Electron probe determination of trace elements in olivine. *X-Ray Spectrom.* **2014**, *43*, 353–358. [CrossRef]

19.　Korolyuk, V.N.; Lavrent'ev, Y.G.; Usova, L.V.; Nigmatulina, E.N. JXA-8100 microanalyzer: Accuracy of analysis of rock-forming minerals. *Russ. Geol. Geophys.* **2008**, *49*, 165–168. [CrossRef]

20.　Lavrent'ev, Y.G.; Korolyuk, V.N.; Usova, L.V.; Nigmatulina, E.N. Electron probe microanalysis of rock-forming minerals with JXA-8100 electron probe microanalyzer. *Russ. Geol. Geophys.* **2015**, *56*, 1428–1436.

21.　Kamenetsky, V.; Kamenetsky, M.; Sobolev, A.; Golovin, A.; Demouchy, S.; Faure, K.; Sharygin, V.; Kuzmin, D. Olivine in the Udachnaya-East kimberlite (Yakutia, Russia): Types, compositions and origins. *J. Petrol.* **2008**, *49*, 823–839. [CrossRef]

22.　Sobolev, N.V.; Logvinova, A.M.; Zedgenizov, D.A.; Pokhilenko, N.P.; Malygina, E.V.; Kuzmin, D.V.; Sobolev, A.V. Petrogenetic significance of minor elements in olivines from diamonds and peridotite xenoliths from kimberlites of Yakutia. *Lithos* **2009**, *1125*, 701–713. [CrossRef]

23.　Skinner, E.M.W. Contrasting Group I and Group II kimberlite petrology: Towards a genetic model for kimberlites. In *Proceedings of The 4th International Kimberlite Conference: Extended Abstracts*; Geology Society of Australia: Perth, Australia, 1989; pp. 528–544.

24.　Moore, A.E. Olivine: A monitor of magma evolutionary paths in kimberlite and olivine melilitites. *Contrib. Mineral. Petrol.* **1988**, *99*, 238–248. [CrossRef]

25.　Moore, A.E. The case for a cognate, polybaric origin for kimberlitic olivines. *Lithos.* **2012**, *128–131*, 1–10. [CrossRef]

26.　Nielsen, T.F.D.; Sand, K.K. The Majuagaa kimberlite dyke, Maniitsoq region, west Greenland: Constraints on an Mg-rich silicocarbonatitic melt composition from groundmass mineralogy and bulk composition. *Can. Mineral.* **2008**, *46*, 1043–1061. [CrossRef]

27.　Bussweiler, Y.; Foley, S.; Prelević, D.; Jakob, J.E. The olivine macrocryst problem: New insights from minor and trace element compositions of olivine from Lac de Gras kimberlites, Canada. *Lithos.* **2015**, *220–223*, 238–252. [CrossRef]

28.　Harte, B. Rock nomenclature with particular reference to deformation and recrystallization textures in olivine-bearing xenoliths. *J. Geol.* **1977**, *89*, 749–753. [CrossRef]

29.　Moore, A.; Costin, G. Kimberlitic olivines derived from the Cr-poor and Cr-rich megacryst suites. *Lithos* **2016**, *258–259*, 215–227. [CrossRef]

30.　Delany, J.S.; Smith, J.V.; Dawson, J.B.; Nixon, P.H. Manganese thermometer for mantle peridotites. *Contrib. Mineral Petrol.* **1979**, *71*, 157–169. [CrossRef]

31.　MacKenzie, J.M.; Canil, D. Composition and thermal evolution of cratonic mantle beneath the central Archean Slave Province, NWT, Canada. *Contrib. Mineral Petrol.* **1999**, *134*, 313–324. [CrossRef]

32.　Schmidberger, S.S.; Francis, D. Nature of the mantle roots beneath the North American Craton: Mantle xenolith evidence from Somerset Island kimberlites. *Lithos* **1999**, *48*, 195–216. [CrossRef]

33.　Gregoire, M.; Bell, D.R.; Le Roex, A.P. Garnet lherzolites from the Kaapvaal Craton (South Africa): Trace element evidence for a metasomatic history. *J. Petrol.* **2003**, *44*, 629–657. [CrossRef]

34.　Boyd, F.R.; Pearson, D.G.; Hoal, K.O.; Hoal, B.G.; Nixon, P.H.; Kingston, M.J.; Mertzman, S.A. Garnet lherzolites from Louwrensia, Namibia: Bulk composition and P/T relations. *Lithos* **2004**, *77*, 573–592. [CrossRef]

35.　Viljoen, F.; Dobbe, R.; Smit, B. Geochemical processes in peridotite xenoliths from the Premier diamond mine, South Africa: Evidence for the depletion and refertilisation of subcratonic lithosphere. *Lithos* **2009**, *112*, 1133–1142. [CrossRef]

36.　Menzies, A.H.; Westerlund, K.; Grutter, H.; Gurney, J.J.; Carlson, J.A.; Fung, A.; Nowicki, T. Peridotitic mantle xenoliths from kimberlites on the Ekati diamond mine property, NWT, Canada: Major element compositions and implications for the lithosphere beneath the central Slave craton. *Lithos* **2004**, *77*, 395–412. [CrossRef]

37. Jakob, W.R.O. Geochemical Aspects of the Megacryst Suite from the Monastery Kimberlite Pipe. Master's Thesis, University of Cape Town, Cape Town, South Africa, 1977; p. 81.

38. Kopylova, M.G.; Russell, J.K.; Cookenboo, H. Petrology of peridotite and pyroxenite xenoliths from the Jericho kimberlite: Implications for the thermal state of the mantle beneath the Slave Craton, northern Canada. *J. Petrol.* **1999**, *40*, 79–104. [CrossRef]

39. Bizzarro, M.; Stevenson, R. Major element composition of the lithospheric mantle under the North Atlantic craton: Evidence from peridotite xenoliths of the Sarfartoq area, southwestern Greenland. *Contrib. Mineral. Petrol.* **2003**, *146*, 223–240. [CrossRef]

40. Pokhilenko, L.N.; Mal'kovets, V.G.; Kuz'min, D.V.; Pokhilenko, N.P. New data on the mineralogy of megacrystalline pyrope peridotite from the Udachnaya kimberlite pipe, Siberian Craton, Yakutian diamondiferous province. *Dok. Earth Sci.* **2014**, *454*, 179–184. [CrossRef]

41. Foley, S.F.; Prelevic, D.; Rehfeldt, T.; Jacob, D.E. Minor and trace elements in olivines as probes into early igneous and mantle melting processes, *Earth Planet. Sci. Lett.* **2013**, *363*, 181–191.

42. Pokhilenko, N.P.; Sobolev, N.V.; Boyd, F.R.; Pearson, D.J.; Shimizu, N. Megacrystalline pyrope peridotites in the lithosfere of the Siberian Platform: Mineralogy, geochemical peculiarities and the problem of their origin. *Russ. Geol. Geophys. 1993 34*, 56–67.

43. De Hoog, J.C.M.; Gall, L.; Cornell, D.H. Trace-element geochemistry of mantle olivine and application to mantle petrogenesis and geothermobarometry. *Chem. Geol.* **2010**, *270*, 196–215. [CrossRef]

44. Köhler, T.P.; Brey, G.P. Calcium exchange between olivine and clinopyroxene calibrated as a geothermobarometer for natural peridotites from 2 to 60 kb with applications. *Geochim. Cosmochim. Acta* **1990**, *54*, 2375–2388.

45. Brey, G.P.; Kohler, T. Geothermobarometry in four-phase lherzolites II. New thermobarometers, and practical assessment of existing thermobarometers. *J. Geol.* **1990**, *31*, 1353–1378. [CrossRef]

46. O'Neill, H.S.C.; Wood, B.J. An experimental study of Fe–Mg partitioning between garnet and olivine and its calibration as a geothermometer. *Contrib. Mineral. Petrol.* **1979**, *70*, 59–70.

47. Gibsher, A.A.; Malkovets, V.G.; Litasov, K.D.; Litasov, Y.D.; Pokhilenko, N.P. Composition of the ordovician lithospheric mantle: Evidence from the study of peridotite xenoliths from camptonite of the Sangilen highland, Central Asian Fold Belt. *Dokl. Earth Sci.* **2010**, *433*, 957–961. [CrossRef]

48. Amundsen, H.E.F.; Griffin, W.L.; O'Reilly, S.Y. The lower crust and upper mantle beneath northwestern Spitsbergen: Evidence from xenoliths and geophysics. *Tectonophysics* **1987**, *139*, 169–185. [CrossRef]

49. Pokhilenko, N.P.; Sobolev, N.V.; Kuligin, S.S.; Shimizu, N. Peculiarities of distribution of pyroxenite paragenesis garnet in Yakutian kimberlites and some aspects of the Siberian craton lithospheric mantle. In *Proceedings of the 7th International Kimberlite Conference*; Red Roof Design: Cape Town, South Africa, 1999; Volume 2, pp. 689–698.

50. Sobolev, N.V.; Yefimova, E.S.; Koptil, V.I. Mineral inclusions in diamonds in the Northeast of the Yakutian diamondiferous province. In Proceedings of the 7th Kimberlite Conference, Cape Town, South Africa, 11–17 April 1999; pp. 816–823.

51. Zinchuk, N.I.; Koptil, V.I. *Typomorphism of Diamonds in the Siberian Craton*; Nedra: Moscow, Russia, 2003.

52. Sobolev, N.V.; Sobolev, A.V.; Tomilenko, A.A.; Kuz'min, D.V.; Grakhanov, S.A.; Batanova, V.G.; Logvinova, A.M.; Bul'bak, T.A.; Kostrovitskii, S.I.; Yakovlev, D.A.; et al. Prospects of search for diamondiferous kimberlites in the northeastern Siberian Platform. *Russ. Geol. Geophys.* **2018**, *59*, 1365–1379. [CrossRef]

53. Sun, J.; Liu, C.Z.; Kostrovisky, S.I.; Wu, F.Y.; Yang, J.H.; Chu, Z.Y.; Yang, Y.H.; Kalashnikova, T.; Fan, S. Composition of the lithospheric mantle in the northern part of Siberian craton: Constraints from peridotites in the Obnazhennaya kimberlite. *Lithos* **2017**, *294*, 383–396. [CrossRef]

54. Howarth, G.H.; Barry, P.H.; Pernet-Fisher, J.F.; Baziotis, I.P.; Pokhilenko, N.P.; Pokhilenko, L.N.; Bodnar, R.J.; Taylor, L.A. Superplume metasomatism: Evidence from Siberian mantle xenoliths. *Lithos.* **2014**, *184–187*, 209–224. [CrossRef]

55. Ionov, D.A.; Doucet, L.S.; Ashchepkov, I.V. Composition of the lithospheric mantle in the Siberian craton: New constraints from fresh peridotites in the Udachnaya-East kimberlite. *J. Petrol.* **2010**, *51*, 2177–2210. [CrossRef]

56. Solovyeva, L.V.; Yasnygina, T.A.; Egorov., K.N. Metasomatic parageneses in deep-seated xenoliths from Udachnaya and Komsomolskaya-Magnitnaya pipes as indicators of fluid transfer through the mantle lithosphere of the Siberian craton. *Russ. Geol. Geophys.* **2012**, *53*, 1304–1323. [CrossRef]

57.  Tychkov, N.S.; Agashev, A.M.; Malygina, E.V.; Nikolenko, E.I.; Pokhilenko, N.P. Thermal perturbations in the lithospheric mantle: Case study of PT equilibrium conditions of xenoliths from the Udachnaya pipe. *Dokl. Earth Sci.* **2014**, *454*, 328–333. [CrossRef]

58.  Harte, B.; Hunter, R.H.; Kinny, P.D. Melt geometry, movement and crystallization in relation to mantle dykes, veins and metasomatism. *Philos. Trans. R. Soc. Lond.* **1993**, *342*, 1–21.

59.  Moore, R.O.; Griffin, W.L.; Gurney, J.J.; Ryan, C.G.; Cousens, D.R.; Sie, S.H.; Suter, G.F. Trace element geochemistry of ilmenite megacrysts from the Monastery kimberlite, South Africa. *Lithos* **1992**, *29*, 1–18. [CrossRef]

60.  Agashev, A.M. Geochemistry of Garnet Megacrysts from the Mir Kimberlite Pipe (Yakutia) and the Nature of Protokimberlite Melts. *Dokl. Earth Sc.* **2019**, *486*, 675–678. [CrossRef]

61.  Burgess, S.R.; Harte, B. Tracing lithosphere evolution through the analysis of heterogeneous G9/G10 garnet in peridotite xenoliths. I: Major element chemistry. In Proceedings of the 7th Kimberlite Conference (Dawson volume), Cape Town, South Africa, 11–17 April 1999.

62.  Burgess, S.R.; Harte, B. Tracing lithosphere evolution through the analysis of heterogeneous G9–G10 garnets in peridotite xenoliths, II: REE chemistry. *J. Petrol.* **2004**, *45*, 609–633. [CrossRef]

63.  Cox, K.G.; Bell, J.D.; Pankhurst, R.J. *The Interpretation of Igneous Rocks*; George Allen Unwin: London, UK, 1979.

64.  Cox, K.G.; Jamieson, B.G. The Olivine-rich Lavas of Nuanetsi: A Study of Polybaric Magmatic Evolution. *J. Petrol.* **1974**, *15*, 269–301. [CrossRef]

65.  Brey, G.P.; Köhler, T.; Nickel, K.G. Geothermobarometry in four-phase lherzolites I. Experimental results from 10 to 60 kb. *J. Petrol.* **1990**, *31*, 1313–1352. [CrossRef]